Article

Study of Power and Trajectory Optimization in UAV Systems Regarding THz Band Communications with Different Fading Channels

Muhammet Ali Karabulut 🆔

Department of Electrical and Electronics Engineering, Kafkas University, Kars 36000, Turkiye;
mali.karabulut@kafkas.edu.tr

Abstract: Researchers are interested in unmanned aerial vehicles (UAVs) because they have many uses in current 5G and future 6G networks and are safer than human-operated vehicles. Terahertz (THz)-band communications are a possible option in 6G for fast communication. THz wireless communication between UAVs is taken into consideration in this work. Different fading channels, which are significant influencing factors in THz communication channel modeling, are used to analyze the performance of UAV communications in THz networks. Consideration must be made to the structure, wireless channel parameters, and transmission characteristics when evaluating the performance of wireless technology. Nakagami-m, Rician, Weibull, and Rayleigh fading channels are all taken into consideration, along with log-normal fading. Moreover, an optimization algorithm for the THz channel is presented, which is meant to minimize transmission power by optimizing the trajectory of uplink and downlink transmissions between the UAV and users. The equations of the UAV locations and the transmission power optimization of each user are derived. Analytical formulations regarding capacity, outage probability, and bit error rate (BER) are generated when performance-influencing factors are taken into account. The analytical analysis is supported by the numerical results that are provided.

Keywords: BER; channel fading; optimization; outage probability; UAV; THz

1. Introduction

Recently, unmanned aerial vehicles (UAVs), generally known as drones, have been utilized in a variety of applications. UAVs are utilized nowadays for a variety of purposes, including data collection, public safety, transportation management, search and rescue, reconnaissance, and surveillance. UAV-assisted communication is a viable strategy for future 6G networks because of the shrinking of communication gear, as well as the flexible deployment and inexpensive cost of UAVs. UAVs are brand-new components of 6G networks and differ dramatically from traditional terrestrial communication nodes in many ways. It is important to highlight that 5G and 6G demand a level of network densification that has never before been necessary. This is extremely difficult and is a problem that aerial and ad hoc communications can directly solve. Through intelligent relaying and the use of broadband in remote locations and cut-off hubs, flying ad hoc networks (FANETs) have the ability to usher in this technological revolution. To support local wireless networks, individual UAVs may function as aerial base stations [1].

There are a number of specific use cases and industries where UAVs have a variety of potential applications in wireless communication networks such as 5G and 6G. For example, in the logistics and transportation sector, UAVs can play an important role thanks to their fast and effective payload capacity. UAVs may be preferred in cases such as the rapid delivery of emergency medical supplies or the rapid shipment of critical parts. In the agricultural sector, UAVs can be an effective tool for phytosanitary monitoring, productivity improvement, and irrigation management. In the field of security and monitoring, UAVs

can be used effectively in issues such as border security, fire monitoring, disaster management, and crime prevention. The media and entertainment industry are another area where UAVs can be used for creative shooting and impressive visual effects. Infrastructure monitoring and maintenance are also areas where UAVs are useful. UAVs can perform unmanned visual inspections of structures such as bridges, power lines, and buildings and detect abnormal conditions. Thanks to their ability to provide easy access to high points, UAVs can facilitate infrastructure-monitoring processes. With the development and improvement of advanced technologies, it is predicted that UAVs will be used more effectively in different industries.

First, because of its large bandwidth, the THz band enables high data rates. To address the need for higher data rates, 6G networks may deliver substantially higher data rates by employing the THz spectrum. Second, within the frequency spectrum, the THz band allows for numerous parallel channels. This capability enables 6G networks to support a huge number of users. Third, because the THz band has minimal latency, it is a feasible option for ultra-low latency applications. THz communication enables real-time engagement by providing a quick and dependable connection. As a consequence of its features, such as fast data rates, large capacity, and low latency, THz band communication is being explored as a viable alternative for 6G networks.

To meet rising bandwidth needs, the frequency band has steadily grown. Terahertz (THz)-band communications [2,3] will be crucial for 6G [4–6] and beyond, even if the millimeter-wave (mmWave)-band [7,8] is already influencing 5G. The final uncharted region of the frequency band is the THz band, which is located between optical bands and microwaves. In order to facilitate THz communications, technologies from both sides are being investigated. All actions beyond the 100 gigahertz (GHz) limit, below which, the majority of known mmWave use cases exist, are classified as THz by RF experts. Opticians, however, refer to any frequency below 10 THz as THz (the far infrared). According to the International Telecommunication Union Radiocommunication Sector, the THz range is 300 GHz to 10 THz and is closely linked to the very high frequency band (300 GHz to 3 THz). THz communications will thus allow for very high bandwidth as well as ultra-low latency communication. Over distances comparable to other applications, 100 Gbps THz networks have previously been demonstrated [9–11]. However, providing mobile communications at the device level and the access level from the perspective of UAV-to-UAV [12], medium-range indoor, vehicular, and device-to-device communications is the pinnacle of THz communications. THz communications may allow for the wireless remoting of human cognition, resulting in pervasive wireless intelligence when paired with other THz-band applications, including precise location sensing and imaging [13].

Fading, which weakens the signal energy and prevents the system from achieving optimum results, is one of the major problems in wireless communication. Since the fading effect of wireless communication channels is caused by unpredictable and random reflection, refraction, attenuation, and scattering events depending on time, statistical models developed on the long-term status of the fading coefficients are used. In the literature, there are many statistical models proposed to model random variables and random processes. Many existing studies suggest that UAVs experience multiple types of fading. The most common models used to model the fading effect of wireless channels are the log-normal, Rayleigh, Rician, Nakagami-m, and Weibull distributions. When there is no line-of-sight (LoS) connection between the receiver and transmitter, Rayleigh fading is utilized to mimic the amplitude of the carrier wave. In transmission routes with high LoS, Nak-agami-m fading is employed. Rician distribution is used in cases of direct transmission between the receiver and transmitter in the wireless communication system or if there is a more dominant transmission path compared with other transmission paths. The shadowing effect on wireless circumstances, when there is a tall building or a high mountain, is mostly modeled using the log-normal distribution. A simple statistical fading model used in wireless communications is called Weibull fading. It has been shown via empirical investigations to be a successful paradigm in both indoor and outdoor settings. One

may establish the bit error rate (BER) based on a certain signal-to-noise ratio (SNR) and channel capacity and finally which channel model best suits the real-time communication situations [14].

UAVs are essential in a wide range of possible wireless applications, such as aerial base stations, to improve energy efficiency, coverage, dependability, and the capacity of wireless networks [15]. One of the many applications of UAVs is UAV relaying, which involves embedding a UAV in a network to create a wireless connection between several nodes despite the lack of a direct communication link between them. This specific application is regarded as an effective method to boost throughput, boost reliability, and expand base station coverage [16]. The utilization of UAVs to assist THz communications is thus a highly advantageous strategy since it increases the likelihood of LoS with ground-user equipment when THz and UAVs are combined [17]. In order to deal with the intense demand on cellular networks with limited spectrum resources, UAV-to-UAV communication is implemented in cellular networks. This enables mobile devices to interact directly with each other under the management of a base station. It is also important to note that the utilization of THz band UAV-to-UAV communication allows for almost real-time processing, uploading, and downloading between two close-proximity user devices [18]. UAV-to-UAV communications in the THz frequency range are taken into consideration in a number of research papers in the literature [19,20]. Based on the discussion above, it is clear that researchers do not prioritize analyzing models that combine THz and UAV technologies' outage probability, average capacity, and bit error rate with various fading channels. Thus, the contributions of this study can be expressed as follows:

- In order to analyze performance, UAVs in THz communication systems are considered in this study.
- Log-normal, Nakagami-m, Rayleigh, Rician, and Weibull channel-fading environments are derived.
- For the optimization of trajectory and to transmit power, an algorithm and theoretical derivations for a UAV system for THz-band communications are presented.
- The capacity, BER, and outage probability of the proposed system are examined using M-QAM and M-PSK modulations.
- The analytical investigation is supported by the numerical results that are provided.

The remainder of this paper is structured as follows: Section 2 features related works. The performance analysis is described in Section 3. Section 4 contains numerical results. Finally, in Section 5, conclusions are presented.

2. Related Works

Recent years have seen a boom in the number of articles published on the THz band, including several tutorials and review papers, as well as technical works. With an abundance of spectrum resources between 0.1 THz and 10 THz, THz-frequency transmission has emerged as a viable short-distance, high-speed, and reliable communication technique for LoS connections in UAV-aided communication networks. Losses due to free-space spreading and molecule absorption are all that LoS channel models need to include. The potential of THz communications to enable mobile communications is notable [21]. UAV communication via the THz channel has been set up in few papers [22,23]. The authors of [22] analyzed the orientation and location estimation capabilities of the THz band between two UAVs based on both position and orientation error boundaries. Using their methodology, they determined that millimeter-level positional accuracy, which is necessary for dispersed sensing, is possible provided that the distance between the receiver and transmitter is sufficiently small. Additionally, their simulations showed that there is no significant improvement in location accuracy beyond a certain point when the bandwidth is increased. The authors of [23] looked at the difficulties in using infrastructure-free, high-data-rate, and low-latency wireless UAV systems in THz communications.

In the literature, a number of stochastic as well as deterministic models addressing the THz channel have been put forward. Refs. [24,25] examined free-space path loss, in

particular, diffraction as well as absorption losses. Ref. [26] offered a condensed method of simulating molecule absorption as a function of frequency and atmospheric circumstances. Gamma–gamma, log-normal, and Weibull distributions were used as traditional channel models by the authors of [27] to quantify the impact of pointing errors. The authors of [28] modeled antenna gains with misalignment as a random variable. A more thorough misalignment model was considered in another study [29] that was developed for free-space optical communications and took air turbulence, receiver detector size, and displacement jitter into consideration. This model was also used by [30,31]. The effectiveness of THz systems is measured in terms of outage probability and connection capacity in all of the models listed above. To the best of the authors' knowledge, none of the available literature has addressed the performance of digital modulation techniques in LoS THz communication channels.

Despite the significance of channel fading in UAV communications, the literature has relatively little research on this topic. The development of UAV networks, for instance, was the subject of [32], but the communication and, in particular, control of UAVs are the main topics of this study. Although the characteristics and needs of aerial networking for civil applications were addressed in [33], the focus of this assessment was on the communication features of UAVs, specifically, network layer designs. On channel modeling, Refs. [32,33] hardly make a mention.

3. Performance Analysis

A wireless communication system that comprises two users and one UAV with channel fading is considered. Figure 1 demonstrates a basic UAV communication system model.
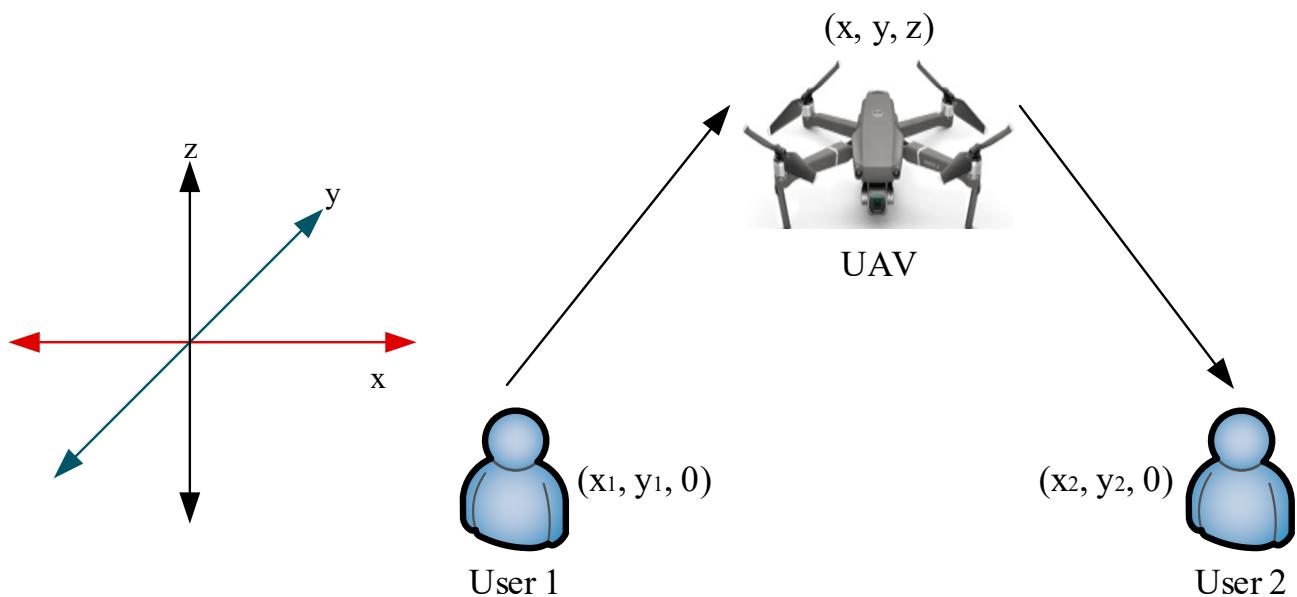
Figure 1. System model.

We outline the wireless THz channels' propagation characteristics. The atmospheric absorption loss and open space path loss together make up the entire loss of the signal that was received. In particular, it is well known that oxygen and water vapor absorb a significant amount of energy in the THz channel [34]. We consider a FANET scenario with a UAV node with a THz communication system. Path loss is incurred by the signal from the source to the destination as a function of frequency and distance, which can be calculated as [35]

$$P_L(d, f) = \left(\frac{c}{4\pi f d} \right)^2 e^{\alpha(f)d}, \tag{1}$$

where d represents the distance between sending and receiving UAV nodes; f is the carrier frequency; c denotes light speed, where the first and second term account for free-space path loss and atmospheric absorption loss, respectively; and $\alpha(f)$ indicates the atmospheric absorption loss coefficient [36]. It is important to calculate the link budget and investigate the correlation between transmission power, distance, BER, and other design characteristics in order to show that a THz wireless communication connection is feasible.

The dominance of the LoS signal is affected by changes in the communication medium, such as building density in the area and the height of the UAV. As a result of these effects, the coefficient of channel-fading values changes.

The UAV's coordinates are indicated by $c = (x, y, z)$, where the coordinates of user 1 and user 2 are provided by $c_1 = (x_1, y_1, 0)$ and $c_2 = (x_2, y_2, 0)$, respectively. It is assumed that the height of the UAV (z) is constant.

The gain in the THz channel between users 1 and 2 and the UAV can be modeled as [37] $h_1 = 1/d_1^2 e^{\alpha(f)d_1}$ and $h_2 = 1/d_2^2 e^{\alpha(f)d_2}$. $d_1(x, y) = \sqrt{(x - x_1)^2 + (y - y_1)^2 + z^2}$ and $d_2(x, y) = \sqrt{(x - x_2)^2 + (y - y_2)^2 + z^2}$ are the distances between the users and the UAV. The uplink transmission rate from user 1 to the UAV may be achieved at [38]

$$R_1^U(x, y) = B_1 \log_2 \left(1 + \frac{P_1 h_0}{B_1 d_1^2 e^{\alpha d_1} \sigma^2} \right), \tag{2}$$

where B_1 indicates the allocated bandwidth to user 1; P_1 designates the transmission power of user 1; Gaussian noise power is shown by σ^2; and h_0 denotes the channel gain at a reference distance, $d_0 = 1$ m. The path loss exponent is represented by α.

Similarly, the achievable rate for the downlink transmission from the UAV to user 2 is

$$R_2^D(x, y) = B_2 \log_2 \left(1 + \frac{P_2 h_0}{B_2 d_2^2 e^{\alpha d_2} \sigma^2} \right), \tag{3}$$

where B_2 denotes the allocated bandwidth to user 2. P_2 indicates the transmission power of the UAV. An algorithm for optimizing x, y, P_1, and P_2 is proposed in Algorithm 1.

Algorithm 1. Optimization of the Transmission Power and Trajectory of the Proposed System

---

Input: x, y, B_1, B_2, P_1, P_2
Calculate Equation (4) with given x, y, B_1, B_2 values
Output: P_1, P_2
Input: B_1, B_2, P_1, P_2
Calculate Equation (7) with given B_1, B_2 values
Output: x, y

3.1. Optimization of Transmission Power

With fixed B_1, B_2, x, and y values, transmission power optimization is formulated as

$$\min \left(\frac{D_1}{B_1 \log_2 \left(1 + \frac{P_1 h_0}{B_1 d_1^2(x,y) e^{\alpha d_1} \sigma^2} \right)} + \frac{D_2}{B_2 \log_2 \left(1 + \frac{P_2 h_0}{B_2 d_2^2(x,y) e^{\alpha d_2} \sigma^2} \right)} \right) \tag{4}$$

$$subject\ to\ \log_2 \left(1 + \frac{P_1 h_0}{B_1 d_1^2(x,y) e^{\alpha d_1} \sigma^2} \right) \geq \frac{D_1}{B_1 E}, \log_2 \left(1 + \frac{P_2 h_0}{B_2 d_2^2(x,y) e^{\alpha d_2} \sigma^2} \right) \geq \frac{D_2}{B_2 E}$$

where D_1 denotes the amount of data that user 1 must send to the UAV. D_2 represents data that the UAV has to deliver to user 1. E represents the user's entire maximum energy. If

(x, y, z) indicates the location of the UAV, the optimal transmission power of user 1, P_1^{*}, can be calculated as

$$P_1^* = -\frac{EB_1(w_1 e^{w_1})'}{D_1 \ln 2} - \frac{B_1 d_1^2 e^{\alpha d_1} \sigma^2}{h_0} \qquad (5)$$

where $w_1 = -\left(EB_1^2 d_1^2 e^{\alpha d_1} \sigma^2 2^{-\frac{B_1 d_1^2 e^{\alpha d_1} \sigma^2 D_1}{h_0 EB_1}} \ln 2\right)/D_1 h_0$. Given the UAV location, (x, y, z), and the bandwidth of the UAV, B_2, the optimal transmission power of the UAV, P_2^{*}, can be written as

$$P_2^* = -\frac{EB_2(w_2 e^{w_2})'}{D_2 \ln 2} - \frac{B_2 d_2^2 e^{\alpha d_2} \sigma^2}{h_0} \qquad (6)$$

where $w_2 = -\left(EB_2^2 d_2^2 e^{\alpha d_2} \sigma^2 2^{-\frac{B_2 d_2^2 e^{\alpha d_2} \sigma^2 D_2}{h_0 EB_2}} \ln 2\right)/D_2 h_0$. Since problem (3)'s objective function is a lessening function with regard to P_q, the optimal P_q^{*} value is the maximum value in the feasible region ($q \in 1, 2$). Based on (3), we find that $\log_2\left(1 + \frac{P_q h_0}{B_q d_q^2 e^{\alpha d_q} \sigma^2}\right)/P_q$ is a decreasing function with regard to P_q. Therefore, P_q^{*} fulfills the following equation: $\frac{D_q}{B_q E} = \log_2\left(1 + \frac{P_q^* h_0}{B_q d_q^2 e^{\alpha d_q} \sigma^2}\right)/P_q^*$.

3.2. Trajectory Optimization

Finding the optimal location for the UAV is the goal in order to reduce the amount of power consumed for transmissions overall, i.e.,

$$\min_{x,y,z} P_{ttp} + P_{tp}$$
$$\text{subject to } \sum_{q=1}^{2} \frac{\iint P_q^{\min}(x,y)dxdy}{P_q} = A \qquad (7)$$

where $P_q^{\min}$ indicates the lowest transmission power ($q \in 1, 2$) that the UAV should arrange for communication with the users at (x, y), and A is a constant. P_{ttp} is the total transmission power of the UAV required to fulfill the data demand of the users. Without sacrificing generality, we assume that the UAV's maximum transmission power is enough to fulfill the user demand for data. P_{tp} denotes the total power of the UAV. $P_q^{\min}$ can be shown as

$$P_q^{\min}(x,y) = B_q d_q^2(x,y) P_L(x,y)(2^{\alpha/B_q} - 1). \qquad (8)$$

P_{ttp} can be calculated as

$$P_{ttp} = \sum_{q=1}^{2} \iint P_q^{\min}(x,y)dxdy. \qquad (9)$$

P_{tp} can be provided by

$$P_{tp} = \sum_{q=1}^{2} \sqrt{(x - x_q)^2 + (y - y_q)^2 + z^2}. \qquad (10)$$

This equation is focused on a high-altitude UAV, where $z^2 > (x - x_q)^2 + (y - y_q)^2$. Equation (7) is clearly a convex function relating to x and y [39]. Initial partial derivatives are set to zero, and the optimal location of the UAV can be provided as

$$
\begin{aligned}
x^* &= \sum_{q=1}^{2} \frac{\iint x B_q d_q^2(x,y) P_L(x,y) (2^{\alpha/B_q} - 1) dx dy}{\iint (2^{\alpha/B_q} - 1) dx dy}, \\
y^* &= \frac{\iint y B_q d_q^2(x,y) P_L(x,y) (2^{\alpha/B_q} - 1) dx dy}{\iint (2^{\alpha/B_q} - 1) dx dy}.
\end{aligned}
\tag{11}
$$

Even though the function of objective (7) is convex with regard to x and y, it is challenging to find a closed-form answer that minimizes a UAV's transmission and mobility power. However, it is easy to discover the numerical solution to (11) using Wolfram Mathematica.

3.3. Average Capacity

In a generalized fading environment, statistical averaging over the probability density function (PDF) of an instantaneous SNR is required to assess the average capacity. However, this PDF is often either unidentified or presented in such a convoluted manner that it does not lend itself to this averaging.

For a signal's (s) transmission bandwidth (BW) and energy over an AWGN channel, Shannon capacity can be expressed as

$$
C_\gamma = B \log_2(1 + \gamma).
\tag{12}
$$

Because C_γ is directly coupled to γ in the Shannon capacity, it may also be seen as an RV (6). By averaging C_γ across the PDF of γ at the receiver's output, it is possible to determine the average channel capacity [40], that is,

$$
\overline{C}_\gamma = B \int_0^\infty \log_2(1 + \gamma) f_\gamma(\gamma) d\gamma.
\tag{13}
$$

3.4. Channel Fading

Fading channel models in THz communication are models that account for the effect of obstacles and losses encountered during the travel of THz signals. These patterns represent various channel losses that result in a decrease in the transmitted signal strength or a change in the signal shape.

They are commonly used elements for selecting different fading channels in the THz band and evaluating their effects on performance. The use of fading profiles, environmental conditions, and frequency-dependent fading criteria is important in improving the efficiency of THz communication and determining the most suitable channels. Based on these criteria, analyses and evaluations of different channels can be made. For this reason, Rayleigh, Rician, Nakagami-m, Weibull, and log-normal fading channels were determined to provide the best communication performance.

3.4.1. Log-Normal Fading

We take into account a system that operates in a quasistatic flat fading channel where the route gains are independent and constant during a frame period. The corresponding PDF is provided by [41]

$$
f_\gamma(\gamma) = \frac{1}{\sigma \gamma \sqrt{2\pi}} e^{\left(-\frac{(\ln \gamma - \mu)^2}{2\sigma^2}\right)}.
\tag{14}
$$

The outage probability, P_{out}, is the likelihood that the received signal's SNR γ will go below the SNR threshold, γ_{th}, which may be expressed as

$$
\begin{aligned}
P_{out} &= P(\gamma < \gamma_{th}) = \int_0^{\gamma_{th}} f_\gamma(\gamma)d\gamma \\
&= \int_0^{\gamma_{th}} \frac{1}{\sigma\gamma\sqrt{2\pi}} e^{\left(-\frac{(\ln\gamma-\mu)^2}{2\sigma^2}\right)} d\gamma = -\frac{1}{2}erf\left(\frac{\log\gamma-\mu}{\sigma\sqrt{2}}\right).
\end{aligned}
\tag{15}
$$

3.4.2. Nakagami-m Fading Channel

The Nakagami-m fading model has a larger spread than the Rician and Rayleigh fading systems and is a channel model that depicts rapid fading over vast distances. The PDF of the SNR γ may be obtained using the γ Nakagami-m distribution as [41]

$$
f(\gamma) = \frac{1}{\Gamma(m)\gamma}\left(\frac{m\gamma}{\overline{\gamma}}\right)^m e^{\left(-\frac{m\gamma}{\overline{\gamma}}\right)}.
\tag{16}
$$

where $\Gamma(.)$ denotes the gamma function, and m represents the parameter determining the distribution's shape. When the Nakagami-m fading parameter is defined as an extremely high value, $(m \to \infty)$, it converges with the AWGN channel. Rayleigh distribution is produced when m is one.

The average SNR of the received signal is provided by

$$
\overline{\gamma} = \frac{\sigma_T G_R G_T \lambda^2}{N_0(4\pi)^2 d^\alpha}.
\tag{17}
$$

G_R and G_T represent the receiving and transmitting antenna gains, respectively. Outage probability can be written as

$$
\begin{aligned}
P_{out} &= P(\gamma < \gamma_{th}) = \int_0^{\gamma_{th}} f_\gamma(\gamma)d\gamma = \int_0^{\gamma_{th}} \frac{1}{\Gamma(m)\gamma}\left(\frac{m\gamma}{\overline{\gamma}}\right)^m e^{\left(-\frac{m\gamma}{\overline{\gamma}}\right)} d\gamma \\
&\cong 1 - e^{\left(-\frac{m\gamma_{th}}{\overline{\gamma}}\right)} \sum_{s=0}^{m-1} \frac{\left(\frac{m\gamma_{th}}{\overline{\gamma}}\right)^s}{s!} = 1 - e^{\left(-\frac{m\gamma_{th}N_0(4\pi)^2 d}{G_R G_T \lambda^2 P_T}\right)} \sum_{s=0}^{m-1} \frac{\left(\frac{m\gamma_{th}N_0(4\pi)^2 d}{G_R G_T \lambda^2 P_T}\right)^s}{s!}.
\end{aligned}
\tag{18}
$$

3.4.3. Rayleigh Fading Channel

Communication is only feasible when signals are reflected, refracted, and scattered as they go from the source to the destination node when there is no LoS between them. A channel whose components are zero-averaged random variables with the same variances has the most detrimental impacts on the error performance of a system; in this case, the envelope of the signal will be distributed according to the Rayleigh distribution. It is possible to determine the receiver's PDF of SNR using a Rayleigh fading channel [41]

$$
f(\gamma) = \frac{1}{\overline{\gamma}} e^{\left(-\frac{\gamma}{\overline{\gamma}}\right)}.
\tag{19}
$$

Outage probability can be expressed as

$$
\begin{aligned}
P_{out} &= P(\gamma < \gamma_{th}) = \int_0^{\gamma_{th}} f_\gamma(\gamma)d\gamma = \int_0^{\gamma_{th}} \frac{e^{\left(-\frac{\gamma}{\overline{\gamma}}\right)}}{\overline{\gamma}} d\gamma \\
&\cong 1 - e^{\left(-\frac{\gamma_{th}}{\overline{\gamma}}\right)} = 1 - e^{\left(-\frac{\gamma_{th}N_0(4\pi)^2 d}{G_R G_T \lambda^2 P_T}\right)}.
\end{aligned}
\tag{20}
$$

3.4.4. Rician Fading Channel

When there is an LoS between S and D or when one transmission line is more dominant than the others, fading coefficients seem to be distributed according to the Rician distribution. The means of the Gaussian processes used to develop this channel model may

differ from zero while also having the same variances. The Rician fading channel system's SNR PDF may be expressed as [40]

$$f(\gamma) = \frac{K+1}{\overline{\gamma}} e^{(-K-\frac{(K+1)\gamma}{\overline{\gamma}})} I_0\left(2\sqrt{\frac{K(K+1)\gamma}{\overline{\gamma}}}\right), \tag{21}$$

where K stands for power distribution between the scattered multipath components and the LoS path. $I_0(.)$ signifies a Bessel function of zero order. $I_0(.)$ is expressed in its broad form as

$$I_\alpha(x) = \sum_{n=0}^{\infty} \frac{K+1}{n!\Gamma(n+1+\alpha)} \left(\frac{x}{2}\right)^{(2n+\alpha)}. \tag{22}$$

Outage probability can be provided by

$$
\begin{aligned}
P_{out} &= P(\gamma < \gamma_{th}) = \int_0^{\gamma_{th}} f_\gamma(\gamma)d\gamma = \int_0^{\gamma_{th}} \frac{K+1}{\overline{\gamma}} e^{(-K-\frac{(K+1)\gamma}{\overline{\gamma}})} I_0\left(2\sqrt{\frac{K(K+1)\gamma}{\overline{\gamma}}}\right)d\gamma \\
&\cong 1 - Q_1\left(\sqrt{2K}, \sqrt{\frac{2(K+1)\gamma_{th}N_0(4\pi)^2 d}{G_R G_T \lambda^2 P_T}}\right).
\end{aligned} \tag{23}
$$

The Marcum-Q function can be written as

$$Q_Z(x,y) = e^{(-\frac{x^2+y^2}{2})} \sum_{k=1-Z}^{\infty} \left(\frac{x}{y}\right)^k I_k(xy). \tag{24}$$

3.4.5. Weibull Fading Channel

The Weibull fading channel system's SNR PDF can be expressed as [41]

$$f(\gamma) = \beta\Gamma\left(1+\frac{1}{\beta}\right)\frac{\gamma^\beta}{\overline{\gamma}\gamma} e^{(-(\frac{\Gamma(1+\frac{1}{\beta})\gamma}{\overline{\gamma}})^\beta)}, \tag{25}$$

where β is the shape factor of distribution. Outage probability can be written as

$$
\begin{aligned}
P_{out} &= P(\gamma < \gamma_{th}) = \int_0^{\gamma_{th}} f_\gamma(\gamma)d\gamma \\
&= \int_0^{\gamma_{th}} \beta\Gamma\left(1+\frac{1}{\beta}\right)\frac{\gamma^\beta}{\overline{\gamma}\gamma} e^{(-(\frac{\Gamma(1+\frac{1}{\beta})\gamma}{\overline{\gamma}})^\beta)}d\gamma \cong 1 - e^{(-(\frac{\Gamma(1+\frac{1}{\beta})\gamma_{th}N_0(4\pi)^2 d}{G_R G_T \lambda^2 P_T})^\beta)}.
\end{aligned} \tag{26}
$$

3.5. Bit Error Rate Analysis

The conditional probability of error that can be achieved with M-PSK and M-QAM at a certain SNR γ value is provided by [41] $P_{\text{BER}}(\gamma) = aQ(\sqrt{b\gamma})$. $Q(.)$ denotes the Gaussian Q function and can be expressed as $Q(x) = (1/\pi) \int\limits_0^{\pi/2} \exp\left(-\frac{x^2}{2\sin^2\theta}\right) d\theta$. BER expressions for M-PSK and M-QAM are presented in Table 1.

Table 1. BER expressions for M-PSK and M-QAM modulations.

Modulation Type	a	b	P_{BER}
M-PSK	$\frac{2}{\log_2 M}$	$2\sin^2\left(\frac{\pi}{M}\right)$	$\frac{aQ(\sqrt{2b\gamma})}{\log_2 M}$
M-QAM	$\frac{4}{\log_2 M}$	$\frac{3}{M-1}$	$\frac{4a}{\log_2 M} \times \sum_{i=0}^{\sqrt{M}/2} (2i-1)\sqrt{2b\gamma \log_2 M}$

The average BER can be computed as follows:

$$\hat{P}_{\text{BER}} = \int_0^\infty P_{\text{BER}}(\gamma) f_\gamma(\gamma) \, d\gamma = \frac{a}{\pi} \int_0^\infty \int_0^{\pi/2} \exp\left(-\frac{b\gamma}{2\sin^2\theta}\right) f_\gamma(\gamma) \, d\gamma d\theta. \tag{27}$$

4. Numerical Results

In this section, the analytical study is verified by numerical results that were obtained using MATLAB and the Wolfram Mathematica program. The numerical expressions were produced by Wolfram Mathematica 13. The values of the parameters used to calculate the findings are shown in Table 2.

Table 2. Value of parameters utilized in the numerical results [5,8,12].

Parameters	Values
f	1–5 THz
G_T, G_R	1, 1
d	0–500 m
σ_R, σ_{Noise}, γ_{th} (dB)	10, -50, 5
α	2

Figure 2 shows the achievable rate (bits/sec/Hz) versus bandwidth (GHz). Increasing the bandwidth provides an increase in the achievable rate. In addition to power consumption, one of the main objectives in designing a communication system is maximizing the achievable rate. However, as bandwidth increases, the achievable rate decreases according to the law of diminishing returns. In fact, the rate of growth in the attainable rate of a wideband-coherent communications system changes as a function of the bandwidth, B. As a result, the possible rate per unit of power often depends on the bandwidth that is available without rising.

Figure 3 provides the required transmission power as a function of bandwidth. As available bandwidth increases, the transmission power optimization value will increase. Also, a wider bandwidth prevents transmission power reduction, especially when the bandwidth is greater than 5 GHz.

Figure 4 shows the average capacity versus the SNR. We can obtain the values of the two distinct frequencies of the various fading channels based on mathematical analysis. The average capacitance rises with increasing frequency. The capacity of the 5 THz system with a Nakagami-m ($m = 2$) channel fading is better than others.

Figure 5 shows the outage probability (P_{out}) versus the transmission distance for different fading channel types. From farther away, the P_{out} increases. The Nakagami-m fading channel has the shortest P_{out} when the distance is short, whereas the Weibull fading channel ($\beta = 2$) has a larger P_{out} than the Rician fading channel ($K = 2$). The P_{out} of Rician fading is higher than that of the log-normal fading channel. The P_{out} of log-normal fading is greater than that of the Rayleigh fading channel. When distance is far—more than 300 m—the Nakagami-m fading channel obtains the highest P_{out}, whereas the Weibull fading channel ($\beta = 2$) achieves a slightly lower P_{out} than the Nakagami-m fading channel. The order of outage probabilities from best to worst is Nakagami-m > Weibull > Rician > log-normal > Rayleigh.

The P_{out} versus SNR values for several fading channels are shown in Figure 6. Increasing the SNR reduces the likelihood of an outage for all fading channel types. Since the SNR rises with signal strength, the probability of an outage decreases. The findings unmistakably demonstrate that the Nakagami-m fading channel's performance has the best performance with the lowest outage probability.

In Figure 7, the number of UAVs is shown versus the likelihood of an outage. The P_{out} grows as the UAV fleet expands. The network architecture rapidly changes as the number of UAVs increases, making communication unstable and increasing the probability of outages. The highest P_{out} is experienced by the model using a Rayleigh fading channel, whereas the model using a Nakagami-m fading channel achieves the smallest amount ($m = 2$).

Figure 8 displays the BER versus SNR values for modulation types under different fading channels. The performance of the system improves as the SNR becomes higher. As a result, the BER goes down. The BER versus SNR value is 2-QAM < BPSK. When compared with the performance of other fading channels, the Nakagami-m fading channel provides superior results for the system.

When the SNR is 20 dB, Figure 9 illustrates the BER vs. the number of UAVs for the various fading channels. As the number of UAVs increases, the BER increases for all fading channel types. More packets will compete for transmission, as there are more UAVs, raising the BER. The maximum BER is attained by the system with a Rayleigh fading channel, while the lowest BER is attained by the system with a Nakagami-m fading channel. When the number of UAVs is low, there is a noticeable difference between the fading channels of the BER, but when the number of UAVs is high, there is a very small difference.
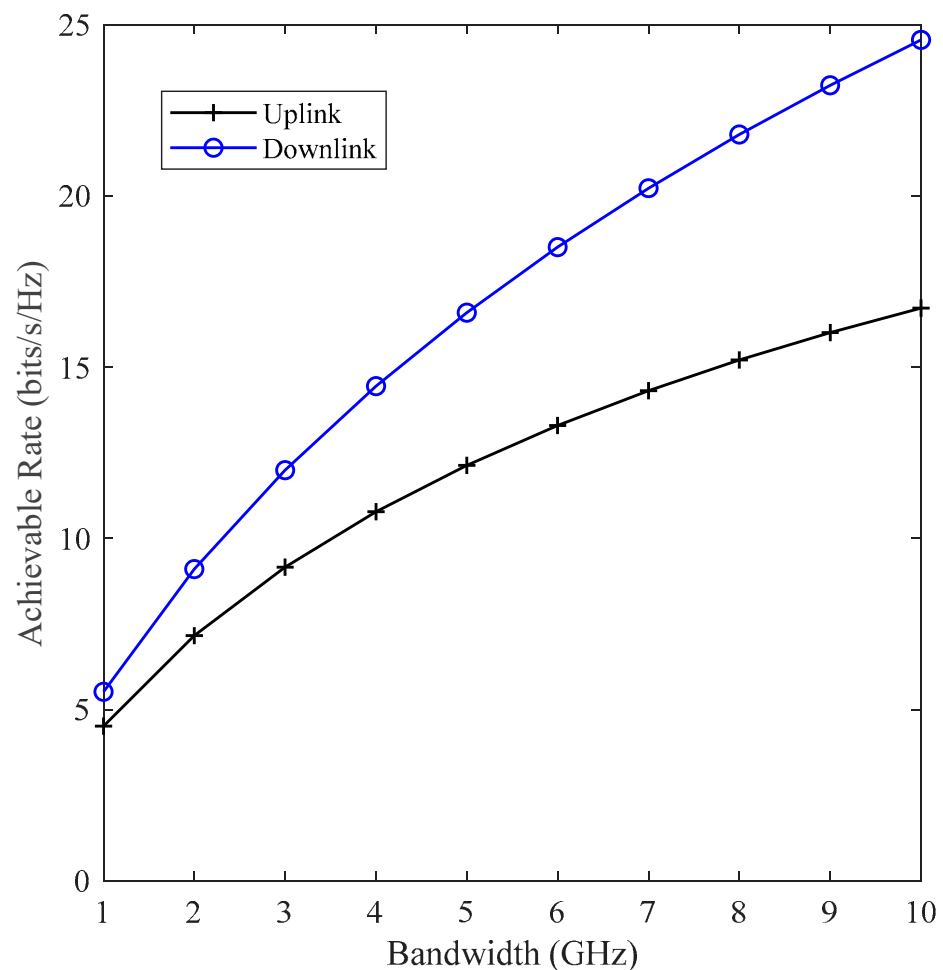
Figure 2. Bandwidth versus achievable rate.
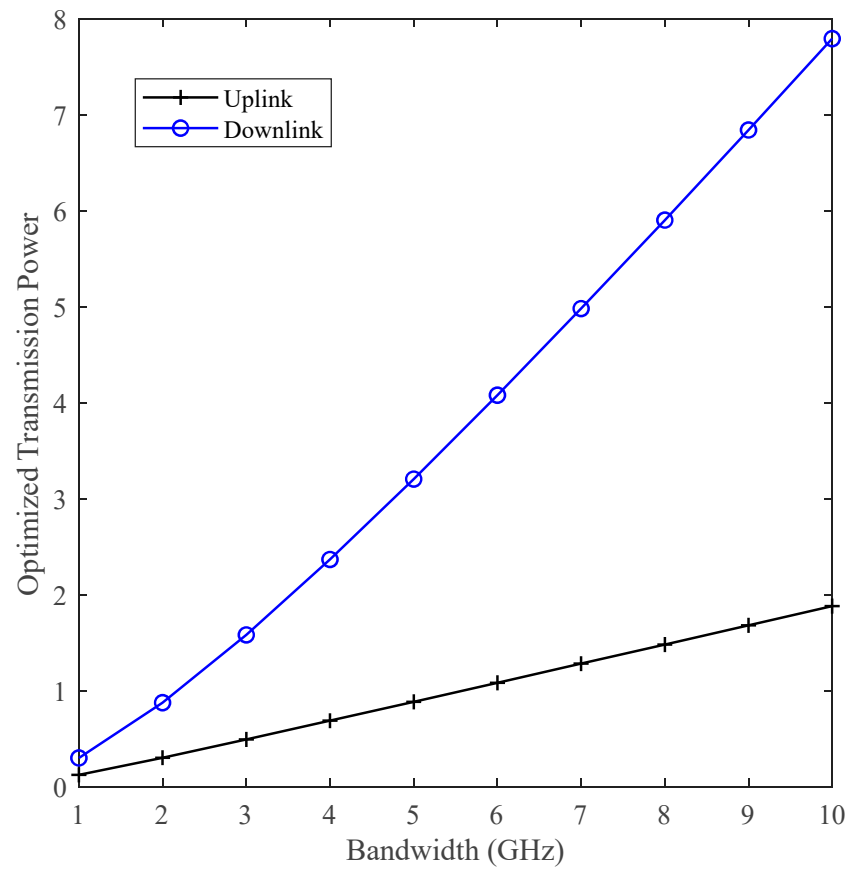
Figure 3. Bandwidth versus transmission power optimization.
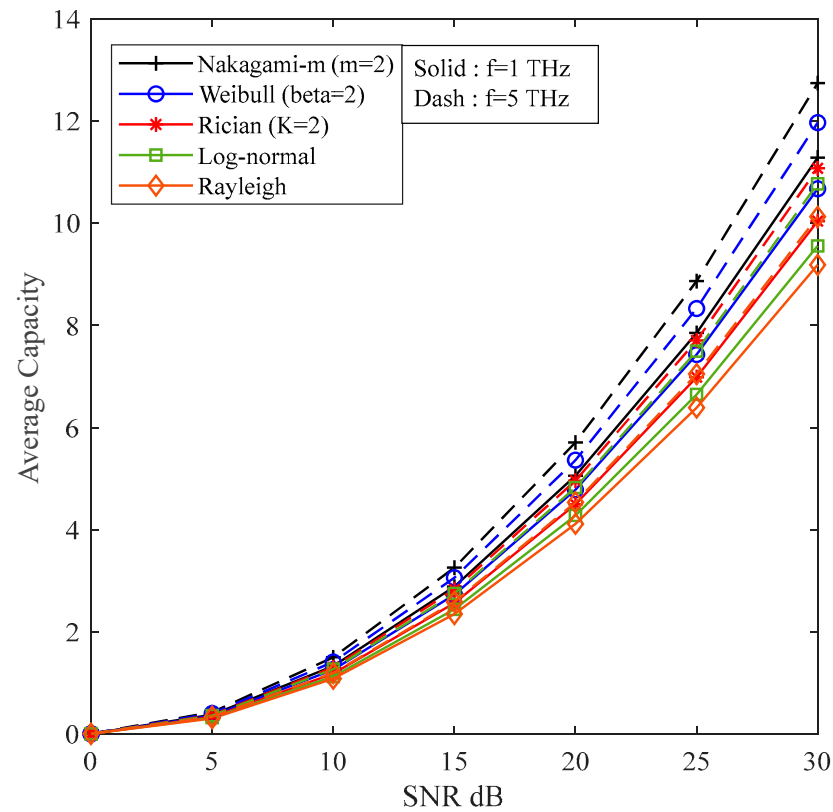
Figure 4. Average capacity versus SNR with different THz frequencies.
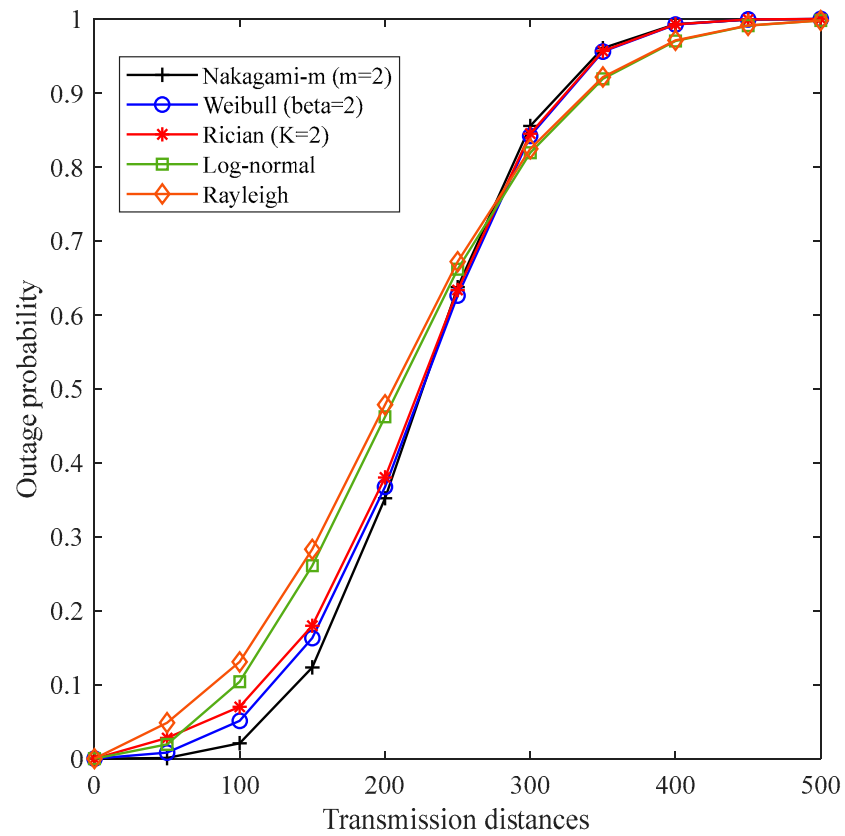
Figure 5. Outage probability vs. transmission distances.
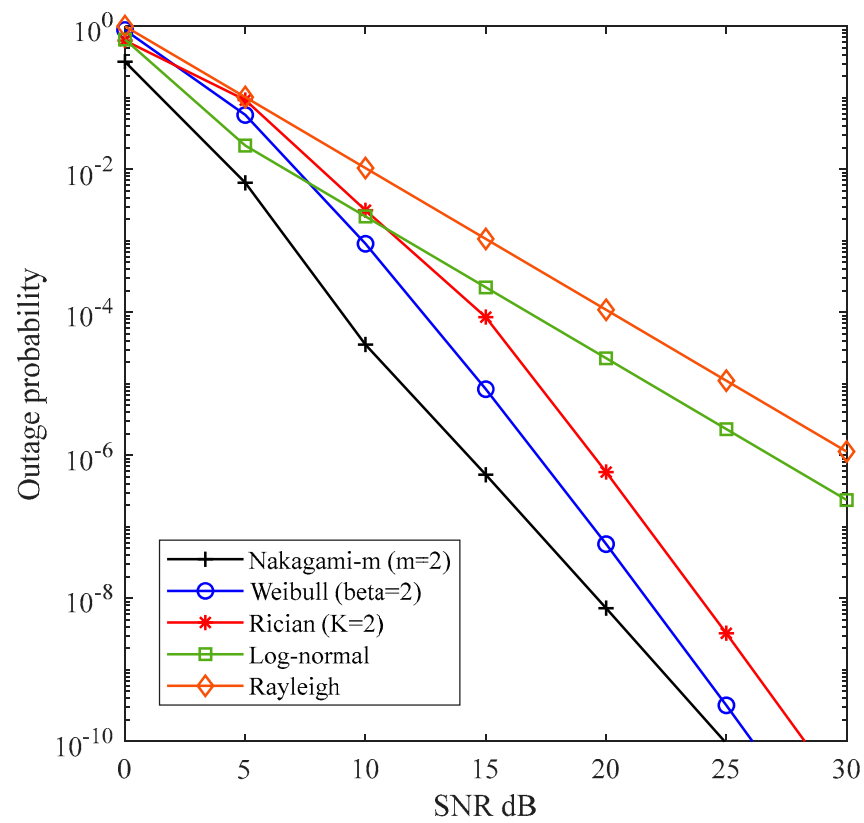
Figure 6. Outage probability versus SNR.
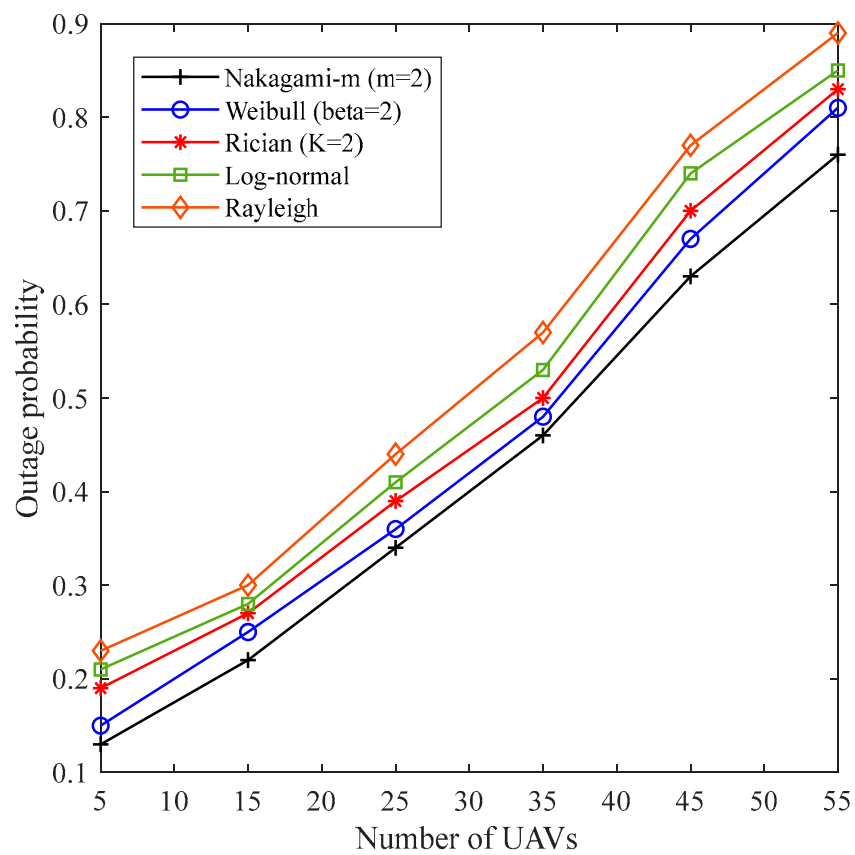
Figure 7. Outage probability versus number of UAVs.
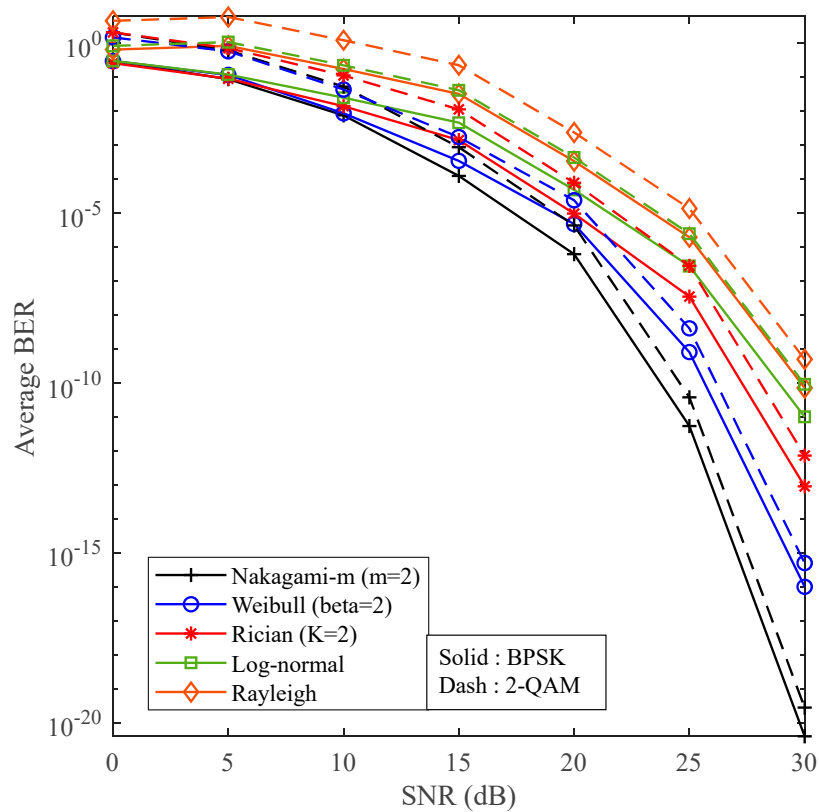
Figure 8. Average BER versus SNR.
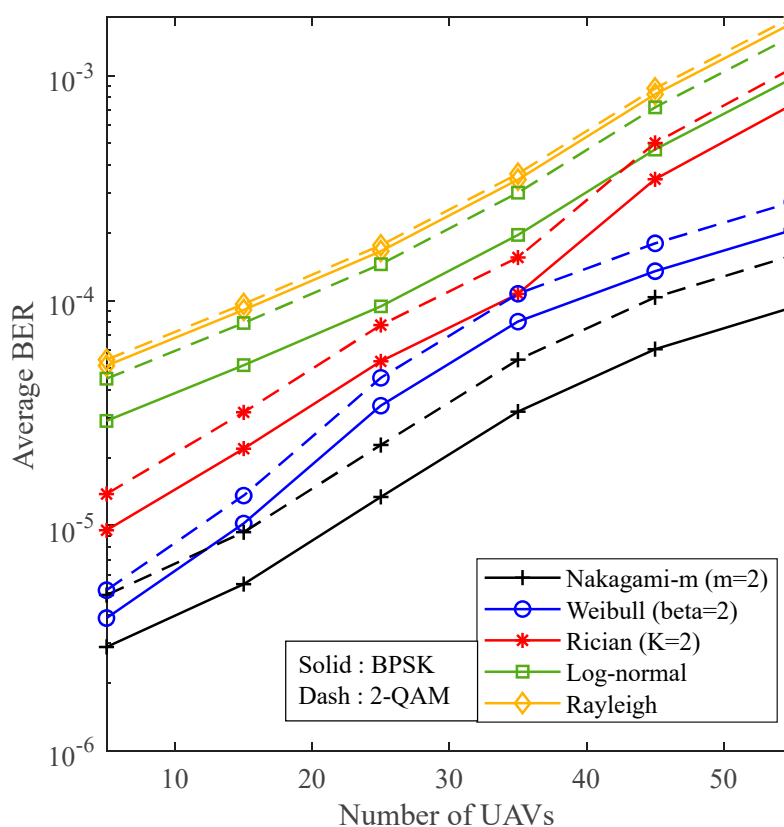
Figure 9. Average BER versus number of UAVs.

5. Conclusions

In this paper, a proposed system for UAV systems for THz communication with different channel-fading types is depicted for the first time. Moreover, a THz channel optimization algorithm is presented with the goal of reducing transmission power by enhancing the uplink and downlink transmission trajectories between the UAV and users. An optimization problem is formulated that searches between the UAV and users while meeting the communication requirements of each user. To solve this problem, an iterative algorithm is proposed that divides the original optimization problem into three sub-problems: the location of the UAV, the power of the users, and the bandwidth of each user in optimizing the three variables. A comprehensive analysis is provided by considering different fading channels. It is observed that the BER and outage probability are relatively high in the low-average SNR, but the BER and outage probability decrease considerably as the average SNR increases. This is observed across all average SNRs and, particularly, in Nakagami-m, where the achieved BER and outage probability are significantly low. Nakagami-m has the best performance compared with other fading channels, that is, Rician, Rayleigh, log-normal, and Weibull. Since they are part of a complete framework that will be helpful in future designs and deployments of new wireless systems, this confirms the value of these additional analytic representations.

Future studies will include further research to gain a clear understanding of the full potential of THz communication schemes for future communication systems in more demanding channel environments. Furthermore, cooperative UAV systems will be discussed, and a study will be provided on how many UAVs are optimal in THz communication to reduce the BER within the scope of co-channel interference models.

Data Availability Statement: No new data were created or analyzed in this study. Data sharing is not applicable to this article.

Conflicts of Interest: The author declares no conflict of interest.

References

1. Shah, A.F.M.S. Architecture of Emergency Communication Systems in Disasters through UAVs in 5G and Beyond. *Drones* **2022**, *7*, 25.
2. Akyildiz, I.F.; Jornet, J.M.; Han, C. TeraNets: Ultra-broadband communication networks in the terahertz band. *IEEE Wirel. Commun.* **2014**, *21*, 130–135.
3. Chen, Z.; Ma, X.; Zhang, B.; Zhang, Y.; Niu, Z.; Kuang, N.; Chen, W.; Li, L.; Li, S. A survey on terahertz communications. *China Commun.* **2019**, *16*, 1–35.
4. Mourad, A.; Yang, R.; Lehne, P.H.; De La Oliva, A. A baseline roadmap for advanced wireless research beyond 5G. *Electronics* **2020**, *9*, 351.
5. Shah, A.F.M.S. A Survey From 1G to 5G Including the Advent of 6G: Architectures, Multiple Access Techniques, and Emerging Technologies. In Proceedings of the IEEE 12th Annual Computing and Communication Workshop and Conference (CCWC), Las Vegas, NV, USA, 26–29 January 2022; pp. 1117–1123.
6. Sarieddeen, H.; Saeed, N.; Al-Naffouri, T.Y.; Alouini, M.-S. Next generation terahertz communications: A rendezvous of sensing, imaging, and localization. *IEEE Commun. Mag.* **2020**, *58*, 69–75.
7. Xiao, M.; Mumtaz, S.; Huang, Y.; Dai, L.; Li, Y.; Matthaiou, M.; Karagiannidis, G.K.; Björnson, E.; Yang, K.; Ghosh, A.; et al. Millimeter wave communications for future mobile networks. *IEEE J. Sel. Areas Commun.* **2017**, *35*, 1909–1935.
8. Rangan, S.; Rappaport, T.S.; Erkip, E. Millimeter-wave cellular wireless networks: Potentials and challenges. *Proc. IEEE* **2014**, *102*, 366–385.
9. Boujnah, N.; Ghafoor, S.; Davy, A. Modeling and link quality assessment of THz network within data center. In Proceedings of the 2019 European Conference on Networks and Communications (EuCNC), Valencia, Spain, 18–21 June 2019; pp. 57–62.
10. Cheng, C.; Sangodoyin, S.; Zajic, A. THz cluster-based modeling and propagation characterization in a data center environment. *IEEE Access* **2020**, *8*, 56544–56558.
11. Nagatsuma, T.; Ducournau, G.; Renaud, C.C. Advances in terahertz communications accelerated by photonics. *Nat. Photonics* **2016**, *10*, 371.
12. Xu, L.; Chen, M.; Chen, M.; Yang, Z.; Chaccour, C.; Saad, W.; Hong, C.S. Joint Location, Bandwidth and Power Optimization for THz-Enabled UAV Communications. *IEEE Commun. Lett.* **2021**, *25*, 1984–1988.
13. Rappaport, T.S.; Xing, Y.; Kanhere, O.; Ju, S.; Madanayake, A.; Mandal, S.; Alkhateeb, A.; Trichopoulos, G.C. Wireless communications and applications above 100 GHz: Opportunities and challenges for 6G and beyond. *IEEE Access* **2019**, *7*, 78729–78757.
14. Akyildiz, I.F.; Kak, A.; Nie, S. 6G and Beyond: The Future of Wireless Communications Systems. *IEEE Access* **2020**, *8*, 133995–134030.
15. Fotouhi, A.; Qiang, H.; Ding, M.; Hassan, M.; Giordano, L.G.; Garcia-Rodriguez, A.; Yuan, J. Survey on UAV cellular communications: Practical aspects, standardization advancements, regulation, and security challenges. *IEEE Commun. Surv. Tutor.* **2019**, *21*, 3417–3442.
16. Wang, H.; Wang, J.; Ding, G.; Chen, J.; Li, Y.; Han, Z. Spectrum sharing planning for full-duplex UAV relaying systems with underlaid D2D communications. *IEEE J. Sel. Areas Commun.* **2018**, *36*, 1986–1999.
17. Pan, Y.; Wang, K.; Pan, C.; Zhu, H.; Wang, J. UAV-assisted and intelligent reflecting surfaces-supported terahertz communications. *IEEE Wirel. Commun. Lett.* **2021**, *10*, 1256–1260.
18. Zhang, S.; Liu, J.; Guo, H.; Qi, M.; Kato, N. Envisioning device-to-device communications in 6G. *IEEE Netw.* **2020**, *34*, 86–91.
19. Abbasi, N.A.; Gomez-Ponce, J.; Kondaveti, R.; Shaikbepari, S.M.; Rao, S.; Abu-Surra, S.; Xu, G.; Zhang, J.; Molisch, A.F. THz Band Channel Measurements and Statistical Modeling for Urban D2D Environments. *IEEE Trans. Wirel. Commun.* **2023**, *22*, 1466–1479.
20. Farrag, S.; Maher, E.; El-Mahdy, A.; Dressler, F. Performance Analysis of UAV Assisted Mobile Communications in THz Channel. *IEEE Access* **2021**, *9*, 160104–160115.
21. Sarieddeen, H.; Alouini, M.-S.; Al-Naffouri, T.Y. An Overview of Signal Processing Techniques for Terahertz Communications. *Proc. IEEE* **2021**, *109*, 1628–1665.
22. Mendrzik, R.; Cabric, D.; Bauch, G. Error bounds for terahertz MIMO positioning of swarm UAVs for distributed sensing. In Proceedings of the 2018 IEEE International Conference on Communications Workshops (ICC Workshops), Kansas City, MO, USA, 20–24 May 2018; pp. 1–6.
23. Guan, Z.; Kulkarni, T. On the effects of mobility uncertainties on wireless communications between flying drones in the mmWave/THz bands. In Proceedings of the IEEE INFOCOM 2019—IEEE Conference on Computer Communications Workshops (INFOCOM WKSHPS), Paris, France, 29 April–2 May 2019; pp. 768–773.
24. Kokkoniemi, J.; Lehtomaki, J.; Juntti, M. A discussion on molecular absorption noise in the terahertz band. *Nano Commun. Netw.* **2016**, *8*, 35–45.
25. Oyeleke, O.D.; Thomas, S.; Idowu-Bismark, O.; Nzerem, P.; Muhammad, I. Absorption, diffraction and free space path losses modeling for the terahertz band. *Int. J. Eng. Manuf.* **2020**, *10*, 54.
26. Kokkoniemi, J.; Lehtomaki, J.; Juntti, M. Simplified molecular absorption loss model for 275–400 gigahertz frequency band. In Proceedings of the 12th European Conference on Antennas and Propagation (EuCAP 2018), London, UK, 9–13 April 2018; pp. 1–5.

27. Taherkhani, M.; Kashani, Z.G.; Sadeghzadeh, R.A. On the performance of thz wireless los links through random turbulence channels. *Nano Commun. Netw.* **2020**, *23*, 100282. [CrossRef]
28. Dabiri, M.T.; Hasna, M. Pointing Error Modeling of mmWave to THz High-Directional Antenna Arrays. *IEEE Wirel. Commun. Lett.* **2022**, *11*, 2435–2439. [CrossRef]
29. Farid, A.A.; Hranilovic, S. Outage capacity optimization for free-space optical links with pointing errors. *J. Light. Technol.* **2007**, *25*, 1702–1710. [CrossRef]
30. Boulogeorgos, A.-A.A.; Papasotiriou, E.N.; Alexiou, A. Analytical performance assessment of thz wireless systems. *IEEE Access* **2019**, *7*, 11436–11453. [CrossRef]
31. Kokkoniemi, J.; Boulogeorgos, A.-A.A.; Aminu, M.; Lehtomaki, J.; Alexiou, A.; Juntti, M. Impact of beam misalignment on thz wireless systems. *Nano Commun. Netw.* **2020**, *24*, 100302. [CrossRef]
32. Gupta, L.; Jain, R.; Vaszkun, G. Survey of important issues in UAV communication networks. *IEEE Commun. Surv. Tutor.* **2016**, *18*, 1123–1152. [CrossRef]
33. Matolak, D.W. Air-ground channels and models: Comprehensive review and considerations for unmanned aircraft systems. In Proceedings of the 2012 IEEE Aerospace Conference, Big Sky, MT, USA, 3–10 March 2012; pp. 1–17.
34. IEEE P802.15 Working Group for Wireless Personal Area Networks (WPANs). (Nov. 2016). Proposal for IEEE 802.15.3D S THz PHY. Available online: https://mentor.ieee.org/802.15/documents?is_group=003d&n=2 (accessed on 17 May 2023).
35. Boulogeorgos, A.-A.A.; Papasotiriou, E.N.; Kokkoniemi, J.; Lehtomaeki, J.; Alexiou, A.; Juntti, M. Performance evaluation of THz wireless systems operating in 275-400 GHz band. In Proceedings of the 2018 IEEE 87th Vehicular Technology Conference (VTC Spring), Porto, Portugal, 3–6 June 2018; pp. 1–5.
36. Recommendation, Attenuation by Atmospheric Gases and Related Effects, Document ITU-R P.676-11. 2008. Available online: https://www.itu.int/rec/R-REC-P.676 (accessed on 17 May 2023).
37. Chaccour, C.; Amer, R.; Zhou, B.; Saad, W. On the reliability of wireless virtual reality at terahertz (THz) frequencies. In Proceedings of the 2019 10th IFIP International Conference on New Technologies, Mobility and Security (NTMS), Canary Islands, Spain, 24–26 June 2019; pp. 1–5.
38. Chen, M.; Yang, Z.; Saad, W.; Yin, C.; Poor, H.V.; Cui, S. A joint learning and communications framework for federated learning over wireless networks. *IEEE Trans. Wirel. Commun.* **2021**, *20*, 269–283. [CrossRef]
39. Mozaffari, M.; Saad, W.; Bennis, M.; Debbah, M. Optimal transport theory for power-efficient deployment of unmanned aerial vehicles. In Proceedings of the 2016 IEEE International Conference on Communications (ICC), Kuala Lumpur, Malaysia, 22–27 May 2016; pp. 1–6.
40. Lee, W.C.Y. Estimate of channel capacity in Rayleigh fading environment. *IEEE Trans. Veh. Technol.* **1990**, *39*, 187–190.
41. Simon, M.K.; Alouini, M.-S. *Digital Communication over Fading Channels*, 2nd ed.; John Wiley & Sons: Hoboken, NJ, USA, 2015.